THE PHOTOGRAMMETRIC RECORD

The Photogrammetric Record 32(160): 377–397 (December 2017)
DOI: 10.1111/phor.12215

OBJECT-BASED CLASSIFICATION OF TERRESTRIAL LASER SCANNING POINT CLOUDS FOR LANDSLIDE MONITORING

ANDREAS MAYR* (andreas.mayr@uibk.ac.at)
University of Innsbruck, Austria

MARTIN RUTZINGER (martin.rutzinger@oeaw.ac.at)
Institute for Interdisciplinary Mountain Research, Austrian Academy of Sciences, Innsbruck, Austria

MAGNUS BREMER (magnus.bremer@uibk.ac.at)
University of Innsbruck, Austria

SANDER OUDE ELBERINK (s.j.oudeelberink@utwente.nl)
University of Twente, Enschede, The Netherlands

FELIX STUMPF (felix.stumpf@agroscope.admin.ch)
Agroscope, Institute for Sustainable Sciences and University of Zürich, Switzerland

CLEMENS GEITNER (clemens.geitner@uibk.ac.at)
University of Innsbruck, Austria

**Corresponding author*

Abstract

Terrestrial laser scanning (TLS) is often used to monitor landslides and other gravitational mass movements with high levels of geometric detail and accuracy. However, unstructured TLS point clouds lack semantic information, which is required to geomorphologically interpret the measured changes. Extracting meaningful objects in a complex and dynamic environment is challenging due to the objects' fuzziness in reality, as well as the variability and ambiguity of their patterns in a morphometric feature space. This work presents a point-cloud-based approach for classifying multitemporal scenes of a hillslope affected by shallow landslides. The 3D point clouds are segmented into morphologically homogeneous and spatially connected parts. These segments are classified into seven target classes (scarp, eroded area, deposit, rock outcrop and different classes of vegetation) in a two-step procedure: a supervised classification step with a machine-learning classifier using morphometric features, followed by a correction step based on topological rules. This improves the final object extraction considerably.

Keywords: erosion, geomorphology, machine learning, object-based point cloud analysis, 3D scene analysis, topology

Introduction and Related Work

The mapping of landslides by close range photogrammetry and remote sensing (Tofani et al., 2013; Scaioni et al., 2014) (collecting topographic information about locations where landslides occur (Rogers and Chung, 2016), as well as the quantification of their extent and volumetric dimension) are essential for building up landslide databases (Zieher et al., 2016). Such databases provide input for process models and landslide risk analysis (Corominas et al., 2014). High-resolution topographic data can be acquired from ground-based or airborne platforms, typically using either laser scanning (Höfle and Rutzinger, 2011) or photogrammetric structure-from-motion image-matching techniques (Westoby et al., 2012).

Terrestrial laser scanning (TLS) is a well-established technique for monitoring landslides and gravitational mass movements in general (Jaboyedoff et al., 2012; Scaioni et al., 2014). TLS produces 3D point clouds with high levels of detail and accuracy, making it particularly suitable for detailed investigations and monitoring tasks at hillslope scales (Ghuffar et al., 2013; Barbarella et al., 2015; Guarnieri et al., 2015). After transformation into a common coordinate system, multitemporal scans can be used to quantify surface changes. However, unstructured TLS point clouds lack semantic information, which is required to interpret the measured changes from a geomorphological point of view.

Landslides produce distinct morphological signatures on the surface (Pike, 1988), which are represented in airborne laser scanning (ALS) digital elevation models (DEMs). Thus, morphometric parameters, such as roughness or curvature, are calculated from ALS DEMs and used for the characterisation or detection of entire landslides, or morphological objects within a landslide (McKean and Roering, 2004; Glenn et al., 2006; Booth et al., 2009; Kasai et al., 2009; Tarolli et al., 2012). Van den Eeckhaut et al. (2012) conceptualise a landslide considering the morphological characteristics of its parts. This conceptualisation is adopted in a rule-set and is used, together with morphometric features and a supervised classification, to map landslides in ALS DEMs.

Object-based image analysis (OBIA) workflows have shown advantages in detection and mapping landslides in optical satellite and airborne imagery (Stumpf and Kerle, 2011; Martha et al., 2012; Kurtz et al., 2014). Such approaches: (i) suppress a noisy ("salt-and-pepper") appearance in classifications of high-resolution data; and (ii) integrate spatial context. For supervised classifications of close-range and remote-sensing data, non-parametric classifiers, such as random forests and support vector machines, have proven successful (Mountrakis et al., 2011; Li et al., 2015; Weinmann et al., 2015; Belgiu and Drăgut, 2016).

In contrast to raster-based approaches, very little attention has been given to 3D object-based analysis for mapping landslides in point clouds and for thorough analysis of their subparts. Most studies that use point clouds for landslide investigations focus on change detection or deformation analysis, without extracting semantic information from the point cloud. For enhanced process understanding of mass movements and secondary erosion, Dorninger et al. (2011) characterise landslides by segmenting ALS and TLS point clouds into planar patches. Monserrat and Crosetto (2008) and Oppikofer et al. (2009) analyse the rotation and translation of individual parts of a point cloud. The automated discretisation of such parts, however, is difficult since the raw 3D point cloud only samples the exposed surface. It provides a detailed geometric representation (X, Y, Z coordinates) but lacks semantic information on discrete geomorphological objects or object classes (such as

landslide scarp or *deposit*). Brodu and Lague (2012) developed a method to classify 3D point clouds of natural scenes based on the dimensionality of point neighbourhoods at multiple scales. They used the knowledge that the geometry of different objects tends to behave uniquely at different scales, making it possible to distinguish between vegetation and rocks, and riparian vegetation from the ground. The surface morphology of landslides and their (vegetated) surroundings is both complex and dynamic, particularly at the detailed scale of TLS surveys. In such complex natural scenes, extracting geomorphologically meaningful objects in several different target classes remains challenging. The challenges relate to the objects' fuzziness in reality as well as the (intra-class) variability and ambiguity (overlap between classes) of their patterns in morphometric feature space.

More research concerning 3D scene analysis and semantic object extraction from point clouds is dedicated to urban environments (Pu et al., 2011; Niemeyer et al., 2014; Guo et al., 2015; Weinmann et al., 2015) and forestry applications (Reitberger et al., 2009; Bremer et al., 2013). In general, object-based point cloud approaches aim at assigning semantic labels to the 3D points by relating them to distinct object classes (such as traffic signs, buildings, façades, roofs, trees and so on). Typically, workflows combine a segmentation of the point cloud into spatially connected units (segments), with subsequent classification of the resulting segments (Rutzinger, 2008). Some recent approaches for point cloud classification are based on an initial over-segmentation, for example, using supervoxels (Lim and Suter, 2009; Ramiya et al., 2016). Often, they utilise spectral information, such as RGB colour values (Li et al., 2016; Ramiya et al., 2016). Spatial contextual reasoning is used in the computer vision and robotics community to classify or interpret 3D point clouds (Hu et al., 2013; Shapovalov et al., 2013).

This paper presents an approach based on point clouds for automatically classifying multitemporal scenes of a hillslope affected by shallow landslides. The first objective is to extract discrete and geomorphologically meaningful objects from TLS point clouds and maximise the objects' consistency throughout the time series. The objects are associated into one of seven target classes (*scarp*, *eroded area*, *deposit*, *rock outcrop* and different classes of vegetation). The second objective is to maintain the spatially accurate, detailed and 3D representation of the scene as a point cloud throughout the analysis. These objectives are pursued by integrating machine-learning methods for supervised classification and a topological rule-set in an object-based analysis workflow. This approach is tested on a series of nine point clouds from a test site with two landslides. To briefly demonstrate the practicability and value of the object extraction, an example of monitoring secondary erosion processes at the level of point cloud objects is also shown.

Test Site

The test site is located in the Schmirn valley (Tyrol, Austria). Two shallow landslide scars (Fig. 1) have existed there since 1965. The larger one of the two landslide scars is approximately 15 to 20 m wide, 30 m long (excluding the rather diffuse runout/depositional zone) and has a maximum depth of two metres. The landslides are still active, with retrogressive erosion at their scarps (that is, clods of material slide or topple downward from the landslide scarp). Occasionally the sliding mass has been reactivated. Moreover, secondary erosion of areas already exposed by runoff, wind or snow movement can occur.

Geologically, the test site is characterised by Bündner Schist covered by regolith. The hillslope is approximately 35° steep, facing south-west and located at about 1700 m elevation. The lower part of the landslides' surroundings is used as a meadow and the upper

FIG. 1. The two landslide scars at the upper part of the test site (Schmirn valley, Tyrol, Austria).

part as an occasional pasture. Larch trees and shrubs are scattered over some sections of the test site. A few rock outcrops exist in the lower part.

METHODS

The automated classification of geomorphological objects is based on segmentation of 3D point clouds into morphologically homogeneous and spatially connected parts. These segments are classified into seven target classes in a two-step classification procedure. The first step is a supervised classification using morphometric features. In a second step, misclassified segments are corrected based on topological rules. In the following sections, each processing step is explained in detail.

Data Acquisition and Preprocessing

The site with its two landslides has been surveyed with a TLS twice a year since 2011. This results in a series of nine TLS point cloud epochs (PC_01 to PC_09) which are used for testing the proposed point cloud classification approach. Two different TLS instruments were used: an Optech Ilris-3D (for epochs PC_01 to PC_05) and a Riegl VZ-6000 (for epochs PC_06 to PC_09). Due to different scanner specifications (such as wavelength, beam divergence and capability to record multiple returns), sensor-dependent differences within the point cloud time series must be assumed.

Scans (with a typical mean point density of about 500 points/m^2) were acquired from two different positions each time to reduce occlusions. The scans were registered via four spherical targets and using an iterative closest point adjustment (ICP; Besl and McKay, 1992). To derive the parameters for the transformation of different epochs' data into a common reference system, ICP was applied only to stable parts of the slope. (Additionally, using deformed parts for this task would impair the registration and consequently impact on point cloud features and change analysis.) To reduce the data volume of the point clouds and homogenise the point density to some extent, 3D block thinning (with 3 cm blocks; similar to an octree filter) was applied, retaining only the point which is closest to each

block centre. These steps, as well as the following analysis workflow, were implemented with Python scripting combined with the free open-source software (FOSS) geographical information system (GIS) SAGA (System for Automated Geoscientific Analysis; Conrad et al., 2015) and the proprietary SAGA add-on Laserdata LIS (Laserdata, 2017).

Point Cloud Features and Segmentation

Local Neighbourhood Features. Point clouds are characterised by computing six features which describe the local morphology around each individual point in the cloud, namely: *2D z range*; *3D/2D density ratio*; *slope*; *standard deviation from a plane*; *omnivariance*; and *geometric curvature*. Both the neighbourhood size and the registration accuracy impact the feature calculation results. To account for multiple scales, three different neighbourhoods were used, of radius 0·2, 0·4 and 1·0 m, for each of the six features (resulting in 18 features). For these three radii, a 3D neighbourhood and a 2D neighbourhood are defined. A 2D neighbourhood is defined as a vertically oriented cylinder of infinite height, centred at the search point. A 3D neighbourhood is defined as a sphere centred at the search point.

The *2D z range* is the difference between the highest and the lowest z value found in the 2D neighbourhood. The *2D/3D ratio* is defined as the number of points found in the 3D neighbourhood, divided by the number of points found in the 2D neighbourhood.

The set of m neighbouring points found by the 3D radius search is used for a principal components analysis (PCA). The point set is encoded into matrix $\mathbf{A}$ with m rows given by:

$$\mathbf{A} = \begin{bmatrix} x_1 - \bar{x} & y_1 - \bar{y} & z_1 - \bar{z} \\ \vdots & \vdots & \vdots \\ x_m - \bar{x} & y_m - \bar{y} & z_m - \bar{z} \end{bmatrix}, \tag{1}$$

from which a 3×3 covariance matrix ($\mathbf{A}^{\mathrm{T}}\mathbf{A}$) is derived as:

$$\mathbf{A}^{\mathrm{T}}\mathbf{A} = \begin{bmatrix} \sum_{i=1}^{m}(x_i - \bar{x})^2 & \sum_{i=1}^{m}(x_i - \bar{x})(y_i - \bar{y}) & \sum_{i=1}^{m}(x_i - \bar{x})(z_i - \bar{z}) \\ \sum_{i=1}^{m}(x_i - \bar{x})(y_i - \bar{y}) & \sum_{i=1}^{m}(y_i - \bar{y})^2 & \sum_{i=1}^{m}(y_i - \bar{y})(z_i - \bar{z}) \\ \sum_{i=1}^{m}(x_i - \bar{x})(z_i - \bar{z}) & \sum_{i=1}^{m}(y_i - \bar{y})(z_i - \bar{z}) & \sum_{i=1}^{m}(z_i - \bar{z})^2 \end{bmatrix}. \tag{2}$$

From this covariance matrix, eigenvectors and eigenvalues are derived. The eigenvector corresponding to the shortest eigenvalue defines the plane fit normal of an orthogonal regression plane and the centroid of the point set defines a point on this plane.

Slope is defined by the angle between the plane normal and a vertically oriented direction vector. The *standard deviation from plane* feature describes the standard deviation of the orthogonal point distance to the local fit plane (defined by the plane normal and the point centroid). The *omnivariance* (λ_0) is a descriptor for the 3D distribution of points in the neighbourhood. It is defined by equation (3) and the three eigenvalues (λ_1, λ_2, λ_3) found by PCA with:

$$\lambda_0 = (\lambda_1, \lambda_2, \lambda_3)^{1/3}. \tag{3}$$

After the normal vectors are defined for each point by PCA, the 3D point neighbourhoods are evaluated in a second program run, allowing comparison of the fitted

normal vector of the search point (n_p) with the normal vectors of all neighbouring points ($n_{np}(j)$) of the set of k point neighbours. The *geometric curvature* (gc) is defined by:

$$gc = \frac{1}{k}\sum_{j=1}^{k} \|n_p - n_{np}(j)\|. \quad (4)$$

Point Cloud Segmentation. For the subsequent object-based analysis, point clouds are partitioned into subsets of spatially connected points that represent morphologically homogeneous (sub-)objects, each belonging to one distinct object class of interest (Fig. 2). This segmentation procedure is a connected component analysis, implemented as seeded region growing with random seed points (the choice of seeds has no notable effect on the final classification results). At this step, three of the point cloud features are assumed to be particularly relevant for separating objects (*3D/2D density ratio*, *omnivariance* and *geometric curvature* for a neighbourhood with a radius of 0·2 m). An unsupervised pre-classification in this morphometric feature space is performed by k-means clustering (Forgy, 1965) with an empirical number of clusters $k = 10$. The nine point cloud epochs are merged into one point cloud before being clustered, to optimise the overall fit of this pre-classification for the entire time series. Subsequently, this point cloud is again split

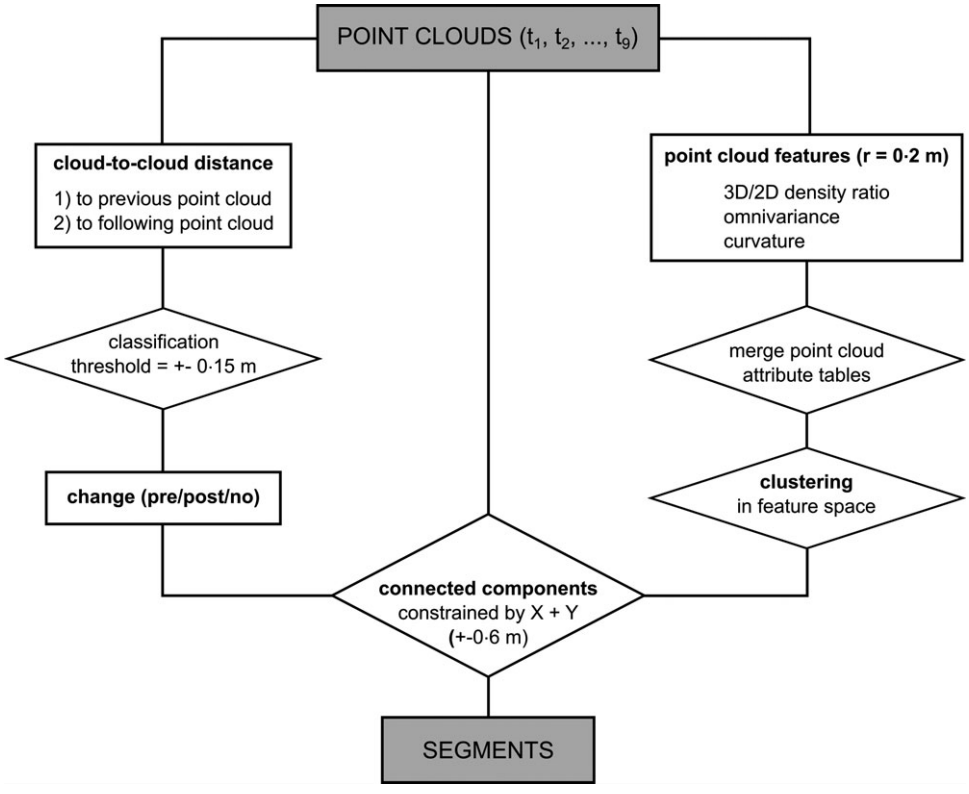

FIG. 2. Point cloud segmentation method.

into the nine epochs and the assigned feature-space clusters are used to constrain the segmentation of each point cloud (separately) in the spatial domain. This aims at creating segments with unique object associations which are semantically consistent for all point cloud epochs.

To keep the segments small and compact, the x and y coordinates additionally constrain the region growing, with a tolerance maximum of $\pm 0{\cdot}6$ m from the seed point allowed. This criterion follows the concept of an initial over-segmentation (Lim and Suter, 2009; Ramiya et al., 2016) as a basis for classification and prevents excessive generalisation of point cloud features.

Moreover, the cloud-to-cloud distances ($distance_{C2C}$) of each point cloud to its predecessor and to its successor point cloud in the time series are calculated (the applied closest point criterion and the resulting distance are influenced by the local point density of each epoch). These distances are used to discriminate areas of change ($distance_{C2C} > 0{\cdot}15$ m) and stable areas ($distance_{C2C} < 0{\cdot}15$ m). This criterion prevents the region growing from including both areas of change and stable areas in the same segment.

Segment Features. For the subsequent object-based analysis (classification of each segment) the 18 local neighbourhood features are aggregated to their mean and standard deviation per segment (resulting in 36 segment features). In addition to the local neighbourhood features, the same principles for feature calculation are applied on a segment basis, where the set of neighbouring points is defined by the set of segment points (this results in seven additional features, yielding 43 in total). As described for the local neighbourhood features, a PCA is performed for the segment points. The three eigenvalues (λ_1, λ_2, λ_3) directly derived by PCA are used as individual segment features. The *slope* and *standard deviation from plane* features are computed as described above. The Sneed–Folk form indices (*SFFI*; Sneed and Folk, 1958) are defined by:

$$SFFI_x = (\lambda_1 - \lambda_2)/(\lambda_1 - \lambda_3) \tag{5}$$

and

$$SFFI_y = \lambda_3/\lambda_1. \tag{6}$$

Supervised Classification of Point Cloud Segments

The classification approach developed for point clouds integrates: (i) a supervised machine-learning classification; and (ii) a classification with topological rules in an object-based analysis framework. The first classification step is a supervised classification using the 43 segment features as predictors (see previous section). Two different machine-learning algorithms are tested, support vector machines (SVMs) and random forests (RF). This step is implemented using *scikit-learn*, a machine-learning package for Python (Pedregosa et al., 2011). The segments represent the samples for training a classifier to predict the class labels in all point clouds. The segment features are standardised by fitting a function to the training data, scaling each feature to a zero mean and unit variance. The same function is used for feature scaling of all other epochs in the time series. To account for heterogeneous class sizes, the class weights are balanced in the training phase by adjusting the weights inversely proportional to the class frequencies in the input data.

One point cloud epoch (PC_07) is manually classified into the seven target classes (*landslide scarp, eroded area, deposit, medium and high vegetation, low grass, high grass, rock outcrop*). Some parts of the scene are difficult to classify with unique labels, both in the 3D point cloud and in the field or on photographs. This concerns, for example, the depositional zone, but also parts of the scarp where no recent erosion has occurred. Accordingly, potential inaccuracies or ambiguities, and a certain degree of subjectivity, in the reference data must be considered for interpretation of the accuracy analyses.

This set of labelled reference segments is split (spatially) into training data (the section containing the larger landslide) and validation data (containing the smaller landslide; Fig. 3). For both machine-learning classifiers used, a few hyper-parameters (parameters not trained in the model) must be specified by the user or by a search procedure. To optimise the classifier and its hyper-parameters, the training data is randomly split into a development set and an evaluation set (random 50% subset for SVM and out-of-bag samples for RF). Using only the development set, a grid search of the parameter space (see Tables I and II) selects the combination of parameter values with the highest score (fraction of correctly classified samples) in a five-fold cross-validation (Olson and Delen, 2008).

Support Vector Classification. Support vector machines (SVMs; Cortes and Vapnik, 1995) are non-parametric statistical learning techniques that are increasingly used for classification tasks, including remote-sensing applications (Ivanciuc, 2007; Mountrakis et al., 2011; van den Eeckhaut et al., 2012). SVM algorithms search for a hyperplane that separates two data classes with the maximum margin around that hyperplane, in other words with the largest possible distance to the instances on both sides. Only the data points that are required to define this margin (support vectors) are used to set up the model. Thus, SVMs can deal with a large number of features and a limited number of training samples. Moreover, the algorithms are relatively tolerant towards irrelevant or redundant features (Kotsiantis, 2007; Mountrakis et al., 2011). A penalty parameter (slack variable) C controls

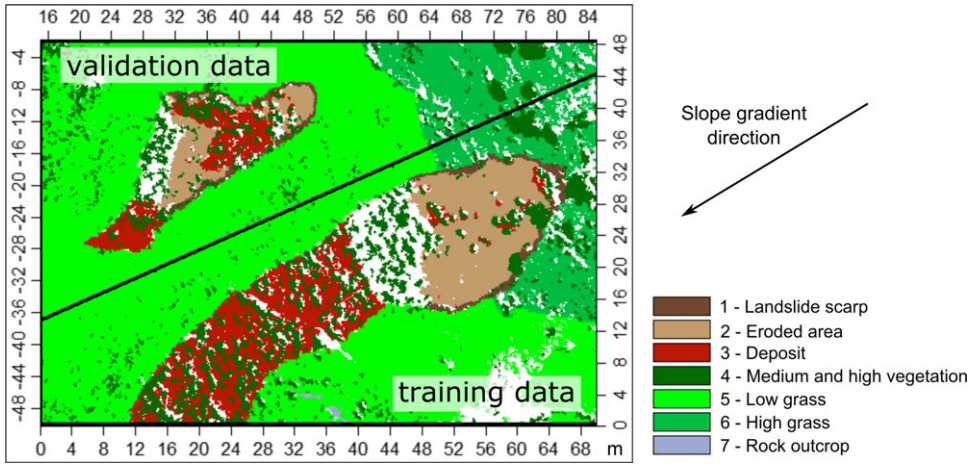

FIG. 3. Manually classified reference point cloud, split (along the black line) into training data and validation data (planimetric view). White areas represent no data, either because of occlusions during scanning or because segments were not classified unambiguously as one specific class.

TABLE I. SVM hyper-parameter optimisation on a random 50% subset of the training data (development set).

Parameter	*Parameter values tested*	*Parameter combination selected*
Kernel	Linear, RBF (radial basis function)	RBF
C	1, 10, 100, 1000	100
γ	0·00001, 0·0001, 0·001, 0·01, 0·1	0·01

the tolerance of the hyperplane and its margin towards training errors. For classification problems where the data is not linearly separable, a kernel function (for example, a radial basis function controlled by the coefficient γ) can map the data to a higher dimensional space (where it is linearly separable). Details and empirically based recommendations on parameter ranges to test can be found in Hsu et al. (2003).

Random Forest Classification. Random forest (RF) is a non-parametric ensemble learner which can efficiently model non-linear relationships, handle a large number of (potentially redundant) features and prevent overfitting (Breiman, 2001; Belgiu and Drăgut, 2016). It aggregates the results of many randomised decision trees by a majority vote for the final results. Each tree is built based on a bootstrap sample of the training instances (subsampling with replacement) and each tree node is split using a user-defined number of randomly selected features (*max_features*; if "sqrt", then *max_features* = sqrt(*n_features*); if "none", then *max_features* = *n_features*). *Max_depth* is the maximum depth of the tree (if "none", then nodes are expanded until all leaves are pure or until all leaves contain less than "min. samples split" samples). *Min_samples_split* is the minimum number of samples required to split an internal node. *Min_samples_leaf* is the minimum number of samples required to be at a leaf node. See scikit-learn documentation (http://scikit-learn.org/stable/index.html) for details and suggested parameter ranges to test.

The data excluded from building a specific tree represent approximately one third of the original data and refer to the out-of-bag (OOB) sample. Passing the OOB data through the specific trees, and aggregating the proportion of misclassifications across all trees, results in an unbiased error estimate of the RF model (Breiman, 2001). This can be used to define an adequate number of trees for the RF classifier. The OOB error rate initially decreases with an increasing number of trees. In this case, it stabilises with the number of trees $n_{estimators} = 700$. With this number of trees other hyper-parameters are optimised (Table II).

Classifier Fitting and Evaluation. The performance of the selected hyper-parameters and the trained classifier is assessed on the evaluation set (random 50% of the training data) that was not used during grid searching and model fitting. Moreover, the overall classifier accuracy (fraction of correctly classified samples) is calculated for the validation dataset

TABLE II. RF hyper-parameter optimisation on a random 50% subset of the training data (development set).

Parameter	*Parameter values tested*	*Parameter combination selected*
max_depth	3, none	None
max_features	sqrt, none	None
min_samples_split	1, 3, 10	3
min_samples_leaf	1, 3, 10	3

(containing the smaller landslide). Additionally, the accuracy metrics *precision* (correctness), *recall* (completeness) and the *F1 score* (Olson and Delen, 2008), per class and overall, are calculated from the true positive (*TP*), false positive (*FP*) and false negative (*FN*) counts as:

$$precision = \frac{TP}{TP + FP} \tag{7}$$

$$recall = \frac{TP}{TP + FN} \tag{8}$$

and

$$F1\ score = \frac{2(precision * recall)}{precision + recall}. \tag{9}$$

Based on the results of this evaluation (see the Results section), the machine-learning classifiers with optimised hyper-parameters are trained on the entire training dataset (containing the larger landslide). Subsequently, the performance of the trained classifiers is evaluated with the validation data (the smaller landslide). Based on this performance, one of the two classifiers is selected to classify all point clouds of the time series (the RF classifier, see Results section).

Landslide Shapes and Rule-based Reclassification of Point Cloud Segments

To correct errors from the supervised classification, topological relationships between landslides and their surroundings are established. Landslide processes are gravitational mass movements and have a clear tendency to move in a downslope direction. The highest part of the resulting landslide form is at the scarp. This logic is used to automatically construct a landslide model from the classified point cloud segments. The number of landslides per scene (n_{LS}) and their approximate minimum separation distance ($dist_{LS}$) must be provided by the user. The landslide models establish a spatial context for the segments within the scene (inside/outside the landslide) and help to employ rules for reclassification.

Extraction of Landslide Shapes. First, all segments labelled as *scarp* are extracted and small and isolated *scarp* segments are removed (as false positives – *FP*s) from the supervised classification. The remaining *scarp* segments are grown to main scarp candidates if they are spatially contiguous. This is a recursive procedure which also considers the segments' elevation relative to the current main scarp candidate. This is based on the assumption that, due to their recurrent geomorphic activity, the top sections of the scarp tend to be the most prominent and least diffuse ones, and thus are recognised more easily than some other parts located lower down. Consequently, the relative elevation criterion allows the scarp-growing procedure to prefer lower segments over higher segments. This proved beneficial because it resulted in more complete main scarp models while rejecting *FP*s above the main scarps which resisted the previous filtering. Such *FP*s result, for instance, from terracettes in the terrain created by livestock trampling. These can have similar morphometric characteristics as parts of the scarp. Finally, only the n_{LS} largest main scarp candidates are extracted. This excludes any remaining *FP*s, such as small rock cliffs misclassified as *scarp*.

In the next step, the downslope area from these main scarps is defined by a raster-based hydrological flow routing (deterministic 8 (D8) algorithm by O'Callaghan and Mark (1984)). The point sets that represent the main scarps and the flow paths are used to construct the approximated landslide polygon outlines as alpha shapes (Edelsbrunner et al., 1983; Figs. 4 and 8). The parameter $dist_{LS}$ is used to discriminate the individual landslides for treatment as separate objects.

Rule-based Reclassification of Point Cloud Segments. Based on simple topological relationships between the labelled point cloud segments and the landslide shapes, misclassified segments are reclassified according to a rule-set (Fig. 5). The rules are inferred from the assumption that *eroded area* and *deposit* do not exist outside the landslide and (undisturbed, low or high) *grass* does not typically occur inside the landslide. The respective misclassified segments are relabelled as the class considered the most likely alternative, also with respect to a visual control of the classification results in all epochs and to the confusion matrix (Fig. 6) which highlights the most severe misclassification types (for the validation data).

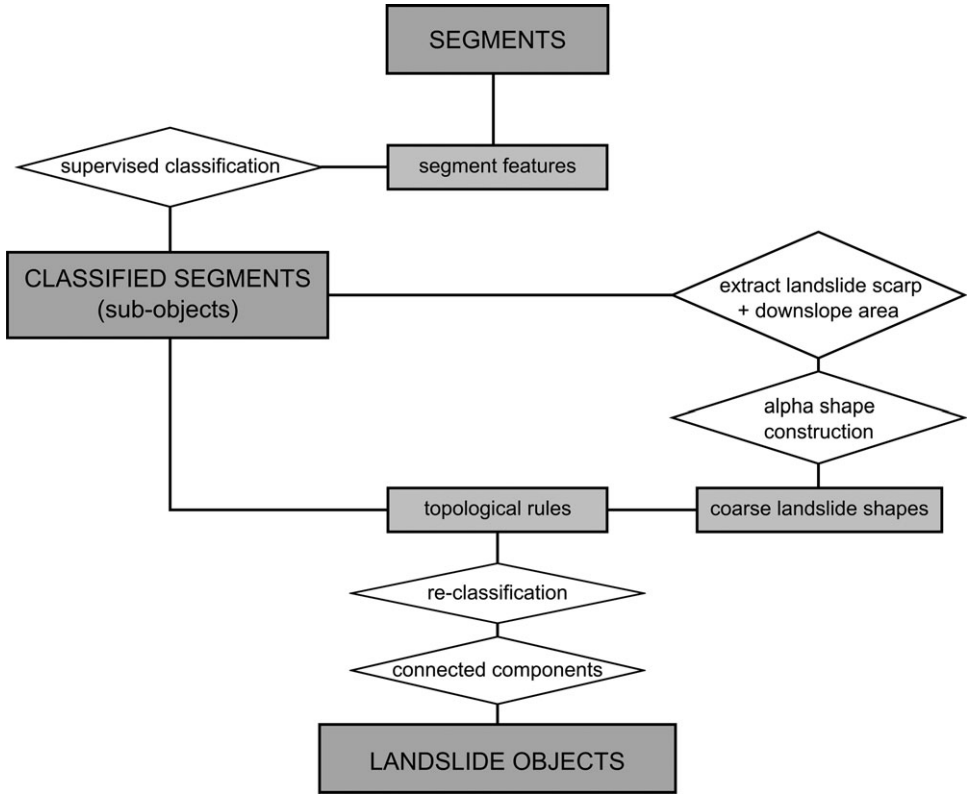

FIG. 4. Two-step classification strategy with supervised classification and rule-based reclassification.

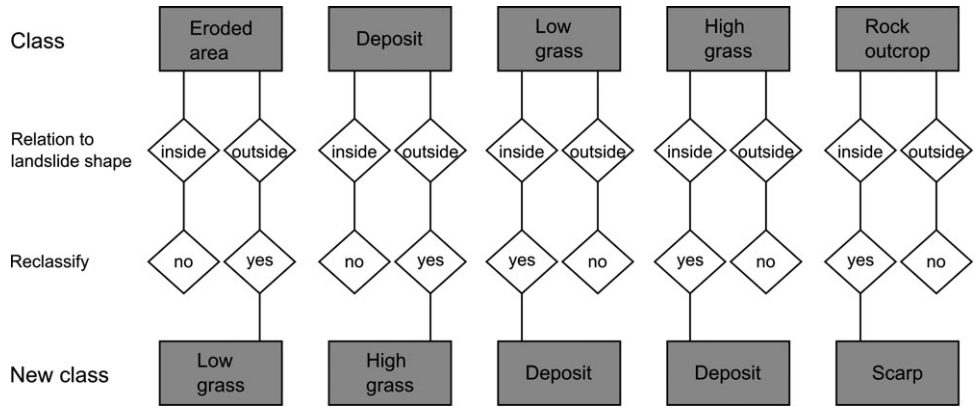

FIG. 5. Topological rules for reclassification.

Extraction of Geomorphological Objects and Change Analysis

Finally, a connected component analysis grows adjacent segments of the same class to discrete scene objects and labels them with a common object identifier (ID). This creates the possibility of analysing changes to specific object classes or to identify changes to individual objects. For example, the cloud-to-cloud distance ($distance_{C2C}$) can be aggregated as a mean and/or standard deviation per object or per class. Moreover, the volume of eroded material can be calculated and, for example, restricted to the scarp (Fig. 9).

RESULTS

Segmentation and Supervised Classification

The segmentation procedure results in a few tens of thousands of segments per epoch, representing the instances to be classified. Around 100 000 points for each point cloud are not grown into any segment and are excluded from further analysis. These points do not meet the criteria for region growing (not enough neighbours (with similar properties) within the search radius) and are almost exclusively points in the vegetation. They can either be classified as such in post-processing or omitted, depending on the application requirements.

Table III shows the per-class accuracy metrics obtained for the training dataset with an SVM and an RF classifier. The model was trained on the development set (random 50% of the training data). The scores are computed on the evaluation set (the other 50% of the training data). In this respect, the overall performance of the two machine-learning classifiers is similar, with RF slightly outperforming SVM for the class *landslide scarp* in terms of precision.

RF also obtained only a slightly higher mean accuracy score for the validation data than SVM (78% versus 76% of correctly classified segments). Fig. 6 compares the results of the two classifiers for the validation data (with the smaller landslide). They accurately recognise *medium and high vegetation* but other classes are prone to errors. *Scarp* is partly misclassified as *deposit*. *Eroded area* tends to be misclassified as *deposit*, *low grass* or *high grass*. *Deposit* is sometimes recognised as *low grass* or *high grass*.

Similar patterns of misclassification are evident from visual inspection of the other epochs. Fig. 7 visualises the results for both classification steps for three different

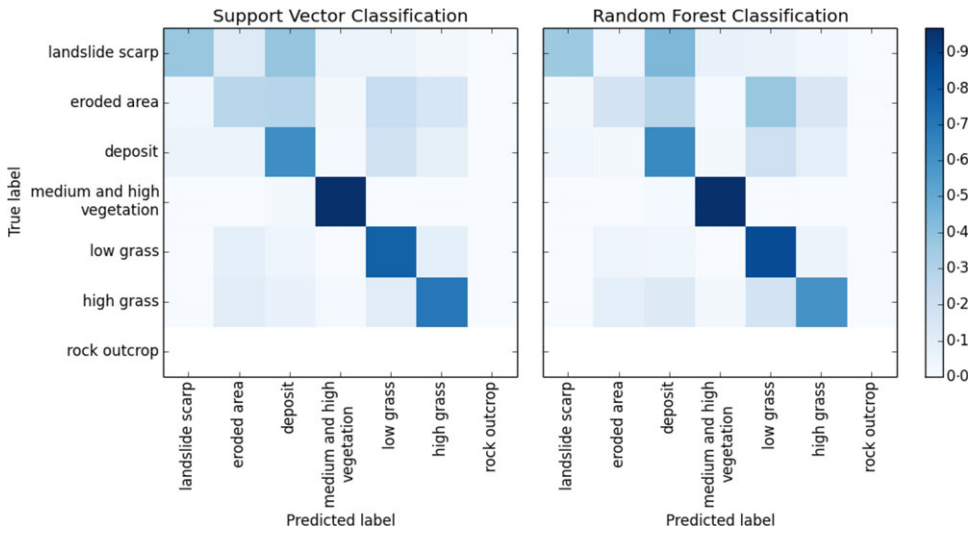

FIG. 6. Confusion matrices for the manually labelled validation data (containing the smaller landslide), normalised by the number of samples in each class. The diagonal elements represent the number of segments for which the predicted label is equal to the true label, while off-diagonal elements are those that are mislabelled by the classifier. *Rock outcrop* (class 7) does not exist in the validation dataset.

TABLE III. SVM and RF classification accuracy metrics (unseen 50% of the training data). See also equations (7) to (9).

Class	*Precision*		*Recall*		*F1 score*		*Segments*
	SVM	*RF*	*SVM*	*RF*	*SVM*	*RF*	*7397 (total)*
1 – Landslide scarp	0·54	0·74	0·69	0·69	0·60	0·71	216
2 – Eroded area	0·59	0·77	0·74	0·60	0·66	0·68	701
3 – Deposit	0·72	0·70	0·79	0·79	0·75	0·74	1106
4 – Medium and high vegetation	0·94	0·92	0·93	0·96	0·93	0·94	2269
5 – Low grass	0·90	0·86	0·76	0·85	0·82	0·85	2325
6 – High grass	0·65	0·73	0·70	0·64	0·68	0·68	734
7 – Rock outcrop	0·71	0·56	0·52	0·83	0·60	0·67	46
Average	0·82	0·82	0·80	0·82	0·81	0·82	

epochs. One of the epochs (PC_04) was acquired with the Optech laser scanner (Fig. 7(a) and (b)), the other two epochs (PC_07 and PC_08) with the Riegl scanner. With respect to the transferability of the trained classifier, the accuracy of the supervised classification is better for the unseen part of the same epoch as where the training data is from (PC_07; Fig. 7(c) and (d)). For other epochs, the classification tends to perform worse but still recognises major parts of the scene correctly. The instrument used for acquisition tends to influence the classification as well (depending on which data was used for training).

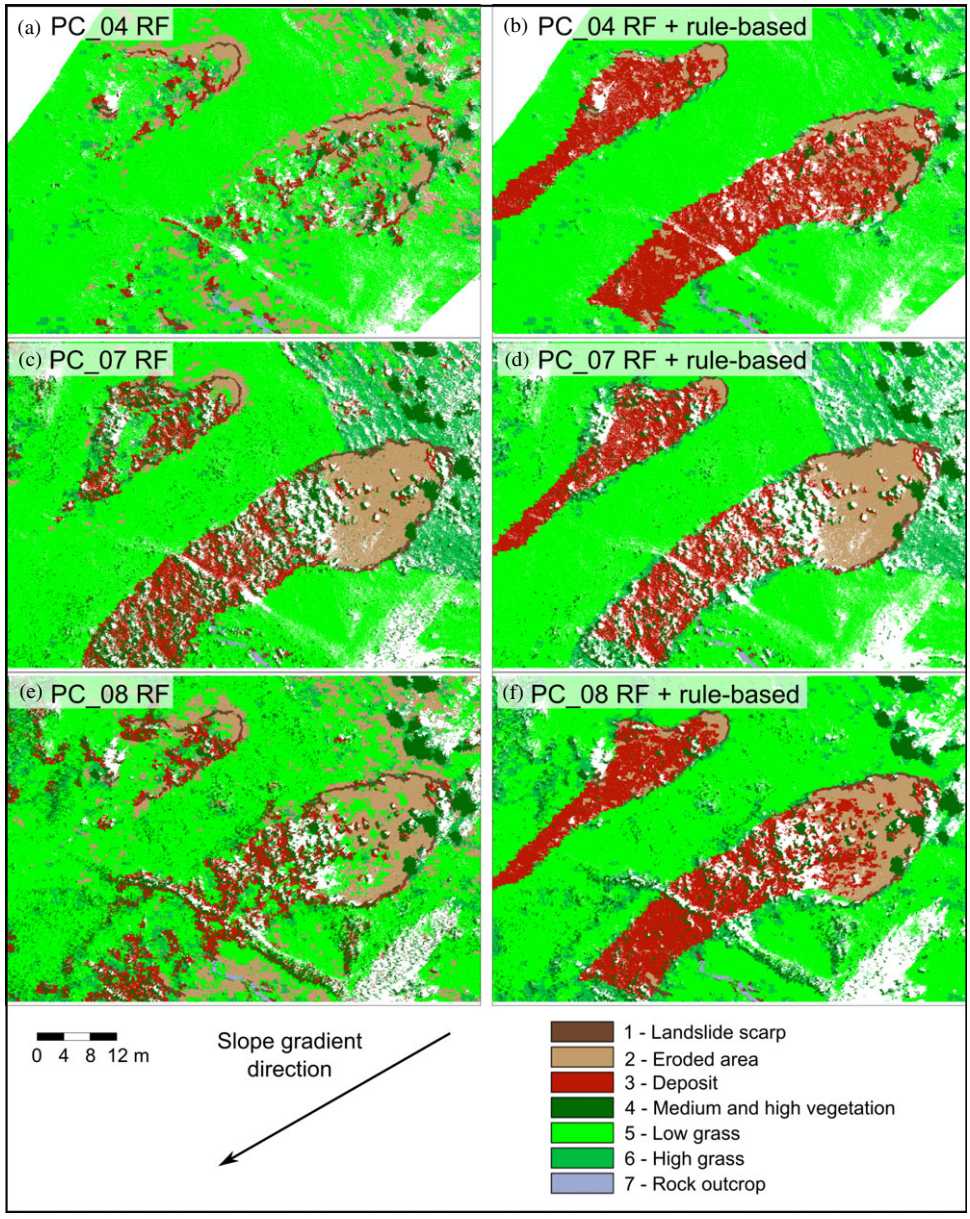

FIG. 7. Planimetric view of three different point cloud epochs (04, 07 and 08) after supervised (RF) classification ((a), (c), (e)) and after rule-based reclassification ((b), (d), (f)).

Rule-based Reclassification

Figs. 7 and 8 show point clouds classified with the RF classifier and the same point cloud reclassified with the topological rule-set and the extracted landslide shapes.

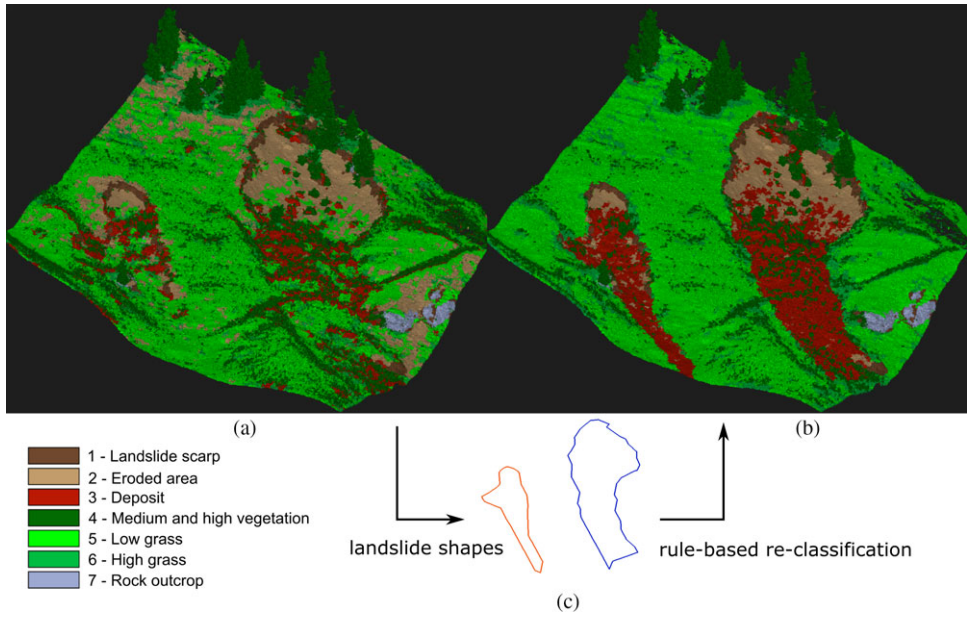

FIG. 8. 3D view of epoch PC_08 after supervised (RF) classification (a) and after rule-based reclassification (b) with the approximated landslide shapes (c) (not to scale).

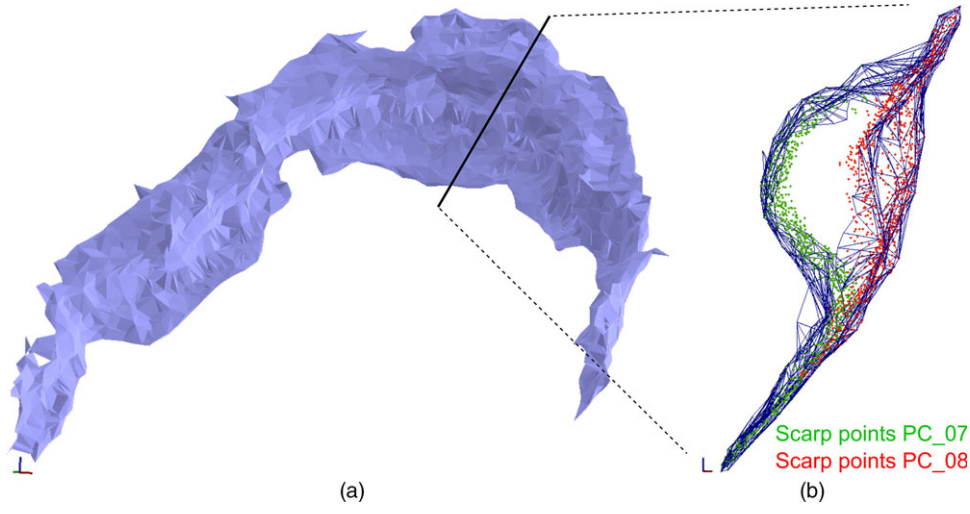

FIG. 9. Scarp erosion between epochs PC_07 and PC_08 (green and red points) represented as 3D alpha shape. (a) Oblique view. (b) Transect through the scarp along the black line.

The differences between epochs are reduced by the second classification step (rule-based reclassification), leading to a more consistent classification of point cloud objects through the time series. Basically, the landslide shapes are reconstructed correctly in all

epochs. In the depositional zones, however, the shapes partly differ. Moreover, the results after the rule-based reclassification tend to overestimate the class *deposit* at the cost of *eroded area* because all segments classified as *grass* are reclassified as *deposit* if they are anywhere within the landslide. On the other hand, the reclassification improves the accuracy score (fraction of correctly classified segments) for certain classes considerably. For the validation data (left, unseen part of epoch PC_07), scores for *deposit* and *high grass* increase from 63% to 77% and from 59% to 71%, respectively.

Object-based Changes

An example of change analysis at the level of landslide objects is presented in Fig. 9. This shows the 3D alpha shapes constructed from the *scarp* points of two successive point clouds. This can be used to visualise and estimate the volume of eroded material that was lost at the scarp between the two scans (approximately 1·7 m^3).

DISCUSSION

The previous sections have presented a point cloud classification and object-extraction approach for landslide monitoring, as well as examples from testing this approach with a time series of nine point clouds from a test site. The results of the accuracy analysis indicate that the two different machine-learning classifiers can perform similarly well for a supervised classification of the scene with morphometric features (overall accuracy metrics differing by a maximum of 2%). Thus, it can be concluded that, in practice, either of the two algorithms – SVM and RF – is suited to accomplishing this first part of the proposed approach, provided that the hyper-parameters are tuned properly and enough training data is available.

For this machine-learning classification on a standard desktop computer, the object-based approach is an advantage because it reduces the number of objects (instances) to be classified by two orders of magnitude (from several million points in the raw point clouds to tens of thousands of segments per epoch). This reduces memory consumption considerably, in particular during the training phase, making a proper grid search for optimisation of hyper-parameters feasible.

Nevertheless, such a supervised classification, restricted to geometric features, has limitations (see the description of common errors above). Some classes of a natural scene are difficult to separate because: (i) their patterns in a morphometric feature space are similar; and (ii) the morphometric signature can be variable within a class. Therefore, the rule-based reclassification, integrating topological relations between objects of a scene, is an important component of the proposed classification approach. This improves the classification accuracy considerably. In particular, errors that are not tolerable from a geomorphological point of view (such as segments outside the landslide misclassified as *eroded area*) can be eliminated.

On the other hand, some classes are overlapping. Most landslide deposits at the test site, for example, are grass-covered, either because clods of turf and soil were displaced and deposited or because of vegetation regrowth already taking place in the less active parts of the landslide. Hence, it depends upon the definition if these parts of the scene should be classified as *grass* or *deposit*.

Reclassifying all initial *grass* segments inside the landslide as *deposit*, results in an overestimation of *deposit* at the cost of *eroded area.* One reason can be that rougher parts

of the eroded area (with relatively large particles at the surface) tend to be misclassified as *grass*. Another reason can be that vegetation succession is already occurring in some parts of the eroded area. Again, this results in an actual overlap of classes and a conflict of definitions, which is also a question of scale. In this respect, the applied topological rules are not capable of accommodating the complexity of the scene in all cases. Improving the rule-set accordingly would require a method to subdivide the landslide shapes into eroded area and depositional zone. This is challenging due to their rather diffuse transition. A soft classification strategy could be an appropriate approach to accommodate the vagueness of these natural objects, also considering constraints to multitemporal object-matching and change analyses.

Inaccuracies of the final classification appear in the lower part of the depositional zones due to incomplete landslide shapes (Fig. 8). Here, the diffuse appearance of the depositional zone, in reality, is limiting both automated and manual delineation. Moreover, limitation of the flow routing at the border of the data's extent can influence landslide shape reconstruction. This can be tolerated, with respect to landslide monitoring, because of the reduced activity in these parts of the scene. The more active parts (which are more prominent in terms of morphology, such as the scarp) are recognised more consistently (Fig. 7).

With regard to its transferability, the supervised classification is validated on an independent dataset (unseen, left part of the scene, containing the smaller landslide). Additionally, the final results from the epoch containing the training data are compared with those from other epochs. Moreover, the presented methods have been tested with point clouds from two different TLS devices. Limitations for transferring the classifier that was trained on one point cloud to other point clouds of the test site can result from: (i) variability in vegetation properties and morphology (phenological state); and (ii) differences in point cloud properties (cf. Fig. 7). The latter are related to the use of two different laser scanners and to different point densities due to inconsistent scan settings. However, in the series of nine point clouds the scarp is recognised and the landslide shapes are constructed correctly. Integration of these key objects with simple topological rules (inferred from basic geomorphological knowledge) is shown to enhance the final classification and object extraction considerably, in particular regarding its consistency through the time series.

Conclusions

This paper has presented an approach to extract geomorphological objects from a time series of TLS point clouds. The experimental results show that the point clouds contain valuable information about the complex morphological characteristics of landslides and their surroundings. Discrete geomorphological objects can be identified and readily used for geomorphological interpretation and process analysis in a multitemporal framework. Thereby, the detailed, 3D geometric information of the point cloud can be jointly used with semantic information. This work demonstrates that this information can be exploited to extract geomorphological objects: (i) automatically; (ii) in a point-cloud-based workflow; and (iii) exclusively using the geometric data. This has several advantages. The high degree of automation makes the analysis reproducible, objective and efficient. This is an important prerequisite for landslide monitoring (with repeated measurements of a scene) on the basis of geomorphologically meaningful and consistent objects. Constraining the analysis to point cloud data representation (no raster conversion) conserves the high level of geometric accuracy and the 3D information

inherent in the original point cloud. An example has demonstrated that this is beneficial for subsequent change analysis to support detailed geomorphological process investigation.

From a methodological point of view, it can be concluded that the combination of a supervised classification with a rule-based reclassification (using simple topological relationships between objects) can yield good results. A machine-learning algorithm (SVM or RF) pre-classified point cloud segments into geomorphologically meaningful object classes. This classification, however, contains certain types of errors, due to ambiguities of certain classes in a purely morphometric feature space. The reclassification step can correct the majority of errors from a machine-learning pre-classification. This increases the fraction of correctly classified segments per class by up to 14%.

The results indicate that the automated classification procedure can be transferred to other landslide scenes with similar morphology and point cloud characteristics (such as point density). Future work should test the transferability to other monitoring sites where landslides occur in a similar natural environment (in terms of morphology and vegetation).

ACKNOWLEDGEMENTS

This work was funded by the Doctoral Fellowship Programme of the Austrian Academy of Sciences. The authors would like to thank all colleagues who supported them during the field campaigns.

REFERENCES

BARBARELLA, M., FIANI, M. and LUGLI, A., 2015. Landslide monitoring using multitemporal terrestrial laser scanning for ground displacement analysis. *Geomatics, Natural Hazards and Risk*, 6(5–7): 398–418.

BELGIU, M. and DRĂGUŢ, L., 2016. Random forest in remote sensing: a review of applications and future directions. *ISPRS Journal of Photogrammetry and Remote Sensing*, 114: 24–31.

BESL, P. J. and MCKAY, N. D., 1992. A method for registration of 3-D shapes. *IEEE Transactions on Pattern Analysis and Machine Intelligence*, 14(2): 239–256.

BOOTH, A. M., ROERING, J. J. and PERRON, J. T., 2009. Automated landslide mapping using spectral analysis and high-resolution topographic data: Puget Sound lowlands, Washington, and Portland Hills. *Oregon. Geomorphology*, 109(3–4): 132–147.

BREIMAN, L., 2001. Random forests. *Machine Learning*, 45(1): 5–32.

BREMER, M., RUTZINGER, M. and WICHMANN, V., 2013. Derivation of tree skeletons and error assessment using LiDAR point cloud data of varying quality. *ISPRS Journal of Photogrammetry and Remote Sensing*, 80: 39–50.

BRODU, N. and LAGUE, D., 2012. 3D terrestrial lidar data classification of complex natural scenes using a multi-scale dimensionality criterion: applications in geomorphology. *ISPRS Journal of Photogrammetry and Remote Sensing*, 68: 121–134.

CONRAD, O., BECHTEL, B., BOCK, M., DIETRICH, H., FISCHER, E., GERLITZ, L., WEHBERG, J., WICHMANN, V. and BÖHNER, J., 2015. System for automated geoscientific analyses (SAGA) v. 2.1.4. *Geoscientific Model Development*, 8(7): 1991–2007.

COROMINAS, J., VAN WESTEN, C., FRATTINI, P., CASCINI, L., MALET, J.-P., FOTOPOULOU, S., CATANI, F., VAN DEN EECKHAUT, M., MAVROULI, O., AGLIARDI, F., PITILAKIS, K., WINTER, M. G., PASTOR, M., FERLISI, S., TOFANI, V., HERVÁS, J. and SMITH, J. T., 2014. Recommendations for the quantitative analysis of landslide risk. *Bulletin of Engineering Geology and the Environment*, 73(2): 209–263.

CORTES, C. and VAPNIK, V., 1995. Support-vector networks. *Machine Learning*, 20(3): 273–297.

DORNINGER, P., SZÉKELY, B., ZÁMOLYI, A. and RONCAT, A., 2011. Automated detection and interpretation of geomorphic features in LiDAR point clouds. *Vermessung & Geoinformation*, 2011(2): 60–69.

EDELSBRUNNER, H., KIRKPATRICK, D. and SEIDEL, R., 1983. On the shape of a set of points in the plane. *IEEE Transactions on Information Theory*, 29(4): 551–559.

FORGY, E., 1965. Cluster analysis of multivariate data: efficiency versus interpretability of classification. *Biometrics*, 21(3): 768–769.

Ghuffar, S., Székely, B., Roncat, A. and Pfeifer, N., 2013. Landslide displacement monitoring using 3D range flow on airborne and terrestrial LiDAR data. *Remote Sensing*, 5(6): 2720–2745.

Glenn, N. F., Streutker, D. R., Chadwick, D. J., Thackray, G. D. and Dorsch, S. J., 2006. Analysis of LiDAR-derived topographic information for characterizing and differentiating landslide morphology and activity. *Geomorphology*, 73(1–2): 131–148.

Guarnieri, A., Masiero, A., Vettore, A. and Pirotti, F., 2015. Evaluation of the dynamic processes of a landslide with laser scanners and Bayesian methods. *Geomatics, Natural Hazards and Risk*, 6(5–7): 614–634.

Guo, B., Huang, X., Zhang, F. and Sohn, G., 2015. Classification of airborne laser scanning data using JointBoost. *ISPRS Journal of Photogrammetry and Remote Sensing*, 100: 71–83.

Höfle, B. and Rutzinger, M., 2011. Topographic airborne LiDAR in geomorphology: a technological perspective. *Zeitschrift für Geomorphologie, Supplementary Issue*, 55(2): 1–29.

Hsu, C.-W., Chang, C.-C. and Lin, C.-J., 2003. *A Practical Guide to Support Vector Classification*. Department of Computer Science, National Taiwan University, Taipei, Taiwan. 16 pages. http://www.csie.ntu.edu.tw/~cjlin/papers/guide/guide.pdf [Accessed: 22nd August 2017].

Hu, H., Munoz, D., Bagnell, J. A. and Hebert, M., 2013. Efficient 3-D scene analysis from streaming data. *IEEE International Conference on Robotics and Automation (ICRA)*: 2297–2304.

Ivanciuc, O., 2007. Applications of support vector machines in chemistry. Chapter 6 in *Reviews in Computational Chemistry*, Volume 23 (Eds. K. B. Lipkowitz and T. R. Cundari). Wiley-VCH, Weinheim, Germany. 484 pages: 291–400.

Jaboyedoff, M., Oppikofer, T., Abellán, A., Derron, M.-H., Loye, A., Metzger, R. and Pedrazzini, A., 2012. Use of LIDAR in landslide investigations: a review. *Natural Hazards*, 61(1): 5–28.

Kasai, M., Ikeda, M., Asahina, T. and Fujisawa, K., 2009. LiDAR-derived DEM evaluation of deep-seated landslides in a steep and rocky region of Japan. *Geomorphology*, 113(1–2): 57–69.

Kotsiantis, S. B., 2007. Supervised machine learning: a review of classification techniques. *Informatica*, 31(3): 249–268.

Kurtz, C., Stumpf, A., Malet, J.-P., Gançarski, P., Puissant, A. and Passat, N., 2014. Hierarchical extraction of landslides from multiresolution remotely sensed optical images. *ISPRS Journal of Photogrammetry and Remote Sensing*, 87: 122–136.

Laserdata, 2017. *Laserdata Software Products*. https://www.laserdata.at/software.html [Accessed: 30th August 2017].

Li, X., Cheng, X., Chen, W., Chen, G. and Liu, S., 2015. Identification of forested landslides using LiDar data, object-based image analysis, and machine learning algorithms. *Remote Sensing*, 7(8): 9705–9726.

Li, Z., Zhang, L., Tong, X., Du, B., Wang, Y., Zhang, L., Zhang, Z., Liu, H., Mei, J., Xing, X. and Mathiopoulos, P. T., 2016. A three-step approach for TLS point cloud classification. *IEEE Transactions on Geoscience and Remote Sensing*, 54(9): 5412–5424.

Lim, E. H. and Suter, D., 2009. 3D terrestrial LIDAR classifications with super-voxels and multi-scale conditional random fields. *Computer-Aided Design*, 41(10): 701–710.

Martha, T. R., Kerle, N., van Westen, C. J., Jetten, V. and Kumar, K. V., 2012. Object-oriented analysis of multi-temporal panchromatic images for creation of historical landslide inventories. *ISPRS Journal of Photogrammetry and Remote Sensing*, 67: 105–119.

McKean, J. and Roering, J., 2004. Objective landslide detection and surface morphology mapping using high-resolution airborne laser altimetry. *Geomorphology*, 57(3–4): 331–351.

Monserrat, O. and Crosetto, M., 2008. Deformation measurement using terrestrial laser scanning data and least squares 3D surface matching. *ISPRS Journal of Photogrammetry and Remote Sensing*, 63(1): 142–154.

Mountrakis, G., Im, J. and Ogole, C., 2011. Support vector machines in remote sensing: a review. *ISPRS Journal of Photogrammetry and Remote Sensing*, 66(3): 247–259.

Niemeyer, J., Rottensteiner, F. and Soergel, U., 2014. Contextual classification of lidar data and building object detection in urban areas. *ISPRS Journal of Photogrammetry and Remote Sensing*, 87: 152–165.

O'Callaghan, J. F. and Mark, D. M., 1984. The extraction of drainage networks from digital elevation data. *Computer Vision, Graphics, and Image Processing*, 28(3): 323–344.

Olson, D. L. and Delen, D., 2008. Performance evaluation for predictive modeling. Chapter 9 in *Advanced Data Mining Techniques*. Springer, Berlin, Germany. 180 pages: 137–147.

Oppikofer, T., Jaboyedoff, M., Blikra, L., Derron, M.-H. and Metzger, R., 2009. Characterization and monitoring of the Åknes rockslide using terrestrial laser scanning. *Natural Hazards and Earth System Sciences*, 9(3): 1003–1019.

Pedregosa, F., Varoquaux, G., Gramfort, A., Michel, V., Thirion, B., Grisel, O., Blondel, M., Prettenhofer, P., Weiss, R., Dubourg, V., Vanderplas, J., Passos, A., Cournapeau, D., Brucher, M., Perrot, M. and Duchesnay, É., 2011. Scikit-learn: machine learning in Python. *Journal of Machine Learning Research*, 12: 2825–2830.

Pike, R. J., 1988. The geometric signature: quantifying landslide-terrain types from digital elevation models. *Mathematical Geology*, 20(5): 491–511.
Pu, S., Rutzinger, M., Vosselman, G. and Oude Elberink, S. J., 2011. Recognizing basic structures from mobile laser scanning data for road inventory studies. *ISPRS Journal of Photogrammetry and Remote Sensing*, 66(6 Supplement): 528–539.
Ramiya, A. M., Nidamanuri, R. R. and Ramakrishnan, K., 2016. A supervoxel-based spectro-spatial approach for 3D urban point cloud labelling. *International Journal of Remote Sensing*, 37(17): 4172–4200.
Reitberger, J., Schnörr, C., Krzystek, P. and Stilla, U., 2009. 3D segmentation of single trees exploiting full waveform LIDAR data. *ISPRS Journal of Photogrammetry and Remote Sensing*, 64(6): 561–574.
Rogers, J. D. and Chung, J.-W., 2016. Mapping earthflows and earthflow complexes using topographic indicators. *Engineering Geology*, 208: 206–213.
Rutzinger, M., 2008. *Object Detection in Airborne Laser Scanning Data in Urban Environments*. Doctoral Thesis, Institute of Geography, University of Innsbruck, Austria. 155 pages.
Scaioni, M., Longoni, L., Melillo, V. and Papini, M., 2014. Remote sensing for landslide investigations: an overview of recent achievements and perspectives. *Remote Sensing*, 6(10): 9600–9652.
Shapovalov, R., Vetrov, D. and Kohli, P., 2013. Spatial inference machines. *IEEE Conference on Computer Vision and Pattern Recognition (CVPR)*: 2985–2992.
Sneed, E. D. and Folk, R. L., 1958. Pebbles in the lower Colorado River, Texas, a study in particle morphogenesis. *Journal of Geology*, 66(2): 114–150.
Stumpf, A. and Kerle, N., 2011. Object-oriented mapping of landslides using random forests. *Remote Sensing of Environment*, 115(10): 2564–2577.
Tarolli, P., Sofia, G. and Dalla Fontana, G., 2012. Geomorphic features extraction from high-resolution topography: landslide crowns and bank erosion. *Natural Hazards*, 61(1): 65–83.
Tofani, V., Segoni, S., Agostini, A., Catani, F. and Casagli, N., 2013. Technical note: Use of remote sensing for landslide studies in Europe. *Natural Hazards and Earth System Science*, 13(2): 299–309.
van den Eeckhaut, M., Kerle, N., Poesen, J. and Hervás, J., 2012. Object-oriented identification of forested landslides with derivatives of single pulse LiDAR data. *Geomorphology*, 173–174: 30–42.
Weinmann, M., Jutzi, B., Hinz, S. and Mallet, C., 2015. Semantic point cloud interpretation based on optimal neighborhoods, relevant features and efficient classifiers. *ISPRS Journal of Photogrammetry and Remote Sensing*, 105: 286–304.
Westoby, M. J., Brasington, J., Glasser, N. F., Hambrey, M. J. and Reynolds, J. M., 2012. "Structure-from-motion" photogrammetry: a low-cost, effective tool for geoscience applications. *Geomorphology*, 179: 300–314.
Zieher, T., Perzl, F., Rössel, M., Rutzinger, M., Meißl, G., Markart, G. and Geitner, C., 2016. A multi-annual landslide inventory for the assessment of shallow landslide susceptibility – two test cases in Vorarlberg, Austria. *Geomorphology*, 259: 40–54.

Résumé

Le laser terrestre à balayage est souvent utilisé pour surveiller des glissements de terrain et autres mouvements gravitaires avec des niveaux de détails et des précisions très poussés. Cependant, les nuages de points laser non structurés ne sont pas porteurs de l'information sémantique qui est requise pour l'interprétation géomorphologique des changements mesurés. L'extraction d'objets significatifs dans un environnement complexe et dynamique constitue un défi en raison du manque de netteté des objets dans le monde réel, ainsi que de la variabilité et de l'ambigüité de leur représentation dans un espace morphométrique. Ce travail présente une approche basée sur les nuages de points pour la classification de scènes multitemporelles sur un versant affecté par des glissements de surface. Les nuages de points 3D sont segmentés en parties morphologiquement homogènes et spatialement connectées. Les segments sont classifiés en sept classes de cibles (escarpement, surface érodée, dépôt, affleurement rocheux et différentes classes de végétation) selon une procédure à deux étapes: une étape de classification supervisée par apprentissage automatique utilisant des caractéristiques morphométriques, suivie d'une étape de correction basée sur des règles topologiques. L'extraction finale d'objets s'en trouve considérablement aléliorée.

Zusammenfassung

Terrestrisches Laserscanning (TLS) wird häufig für ein geometrisch hochgenaues und detailliertes Monitoring von Rutschungen und anderen gravitativen Massenbewegungen verwendet. Die unstrukturierten TLS Punktwolken enthalten allerdings nicht die semantische Information, die für die geomorphologische Interpretation von gemessenen Änderungen benötigt wird. Schwierigkeiten bei der Extraktion von sinnhaften Objekten in einer komplexen und veränderlichen Umgebung ergeben sich durch die Unschärfe der Objekte in der Realität sowie durch ihre teils mehrdeutigen Muster in einem morphometrischen Merkmalsraum. In diesem Artikel wird ein punktwolken-basierter Ansatz zur Klassifizierung multi-temporaler Szenen vorgestellt. Die Szenen bilden einen von flachgründigen Rutschungen betroffenen Hang ab. Die 3D Punktwolken werden in morphologisch homogene, räumlich zusammenhängende Bereiche segmentiert. Diese Segmente werden in einem zweistufigen Verfahren sieben Zielklassen (Anrisskante, Abtragsfläche, Ablagerungsbereich, Felswand sowie verschiedene Vegetationsklassen) zugeordnet: auf eine überwachte Klassifizierung anhand morphometrischer Merkmale folgt eine Korrektur mittels topologischer Regeln. Diese Korrektur verbessert die abschließende Objektextraktion deutlich.

Resumen

El escaneo láser terrestre (TLS) se usa a menudo para monitorear deslizamientos de tierra y otros movimientos de masa gravitacional con gran detalle geométrico y precisión. Sin embargo, las nubes de puntos TLS no estructuradas carecen de la información semántica que se requiere para interpretar geomorfológicamente los cambios medidos. La extracción de objetos en un entorno complejo y dinámico es un reto debido ambigüedad de los objetos, a la variabilidad y ambigüedad de sus patrones en un espacio de características morfométricas. Este trabajo presenta un enfoque basado en la nube de puntos para clasificar escenas multi-temporales de una ladera afectada por deslizamientos superficiales. Las nubes de puntos 3D se segmentan en partes morfológicamente homogéneas y espacialmente conectadas. Estos segmentos se clasifican en siete clases objetivo (área escarpada, área erosionada, depósito, afloramiento rocoso y diferentes clases de vegetación) en un procedimiento de dos etapas: una etapa de clasificación supervisada con un clasificador de aprendizaje automático utilizando características morfométricas, seguida de un paso de corrección basado en reglas topológicas. Esto mejora considerablemente la extracción final del objeto.

摘要

地面激光扫描仪(TLS)经常应用于监测滑坡和其他地表形变,可以提供高精度丰富的几何细节。然而,非结构化的TLS点云缺乏语义信息,而这是在对测量所得变化进行地貌学解译时所必需的。在复杂且动态的环境中提取有意义的目标物体是具有挑战性的,因为目标在真实世界中具有模糊性,而且在形态特征空间中的模式亦多变和模棱两可。本研究提出了一种基于点云的方法,将由浅层滑坡所影响的山坡进行多时态的场景分类。将三维点云分割成形态上同质且空间连续的区块。这些区块包含七个目标类(陡坡、侵蚀区、沉积区、岩石露头、以及不同类型的植被),过程分为两阶段:监督式分类,及使用形态特征的机器学习分类,并继以基于拓扑关系的改正步骤。本方法显著地改善了对最终目标物体的提取。